Elastic Launch Vehicle Response to Sinusoidal Gusts

LARS E. ERICSSON,* J. PETER READING,† AND ROLF A. GUENTHER‡
Lockheed Missiles & Space Company Inc., Sunnyvale, Calif.

An analytic theory is presented that can predict the gust penetration loads and associated elastic vehicle response of Apollo-Saturn launch vehicles penetrating sinusoidal gusts. It is shown that the neglect of separated flow effects in existing theories gives highly unrealistic and often unconservative predictions of the gust penetration loads and elastic vehicle response. The presented theory includes the effects of separated flow and associated convective time lag, and by accepting static experimental data as an input, the theory provides realistic predictions of gust penetration loads and elastic vehicle response. The analysis shows that the elastic vehicle resonant response to sinusoidal gusts is large and may be cause for concern on launch vehicles of the Apollo-Saturn class.

Nomenclature

a = speed of sound, m/sec
A = cross-sectional area, m^2
B = parameter, $B = (\rho U^2/2)S/\tilde{m}$
c = reference length (maximum body diameter) m
C_{ni}, C_n = summation coefficients defined in Eqs. (16, 17, and 17a)
D = aerodynamic damping derivative defined in Eq. (9)
E_n, F_n = summation coefficients defined in Eqs. (23) and (24)
f = gust function of inertial space coordinate X
g, G = gust functions of time defined in Eqs. (11–13)
i = the imaginary number $(-1)^{1/2}$
I = momentum, kg-sec
K = aerodynamic stiffness derivative defined in Eq. (9)
L_b, L_b^*, L_g = body length, body characteristic length, and gust wavelength, m
L = lift kg coefficient $C_L = L/(\rho U^2/2)S$
$\tilde{m}$ = generalized mass, kg-sec^2/m
$M = U/a$ = Mach number
M_A = axial force generated pitching moment, kg-m coefficient $C_{MA} = M_A/(\rho U^2/2)Sc$
M, N = maximum number of summation terms, Eq. (9)
N = normal force, kg: coefficient $C_N = N/(\rho U^2/2)S$
$P(t)$ = generalized force, kg or kg-m/m, defined in Eq. (2)
$q(t)$ = amplitude, m, of normalized bending deflection, $\phi(x)\,q(t)$
$\hat{q}(s)$ = Laplace variable, $\hat{q}(s) = \int_0^\infty e^{-st} q(t)dt$
r = body (cross section) radius, m
$S = \pi c^2/4$ = reference area, m^2
S^* = critical Strouhal number, Eq. (27)
t, t', t^* = time, sec
U = vehicle velocity, m/sec
W_g = gust velocity normal to vehicle path, m/sec
X = inertial space coordinate, m (Fig. 2)
x = body fixed coordinate, m (Fig. 2)
Y = inertial space coordinate, m (Fig. 2)
y = body fixed lateral deflection due to bending, m (Fig. 2)
α = angle of attack, rad or deg
β = angular measure of lateral translation, rad or deg
Δ = amplitude or increment
ε = closeness-to-resonance parameter, Eq. (21)
ζ = structural damping, fraction of critical
ζ_T = total damping, fraction of critical, Eq. (12)
θ = bending body slope, radians or degrees
κ = time lag parameter defined in Eq. (5)
v_{max} = maximum number of sinusoidal gust cycles of given wavelength (Fig. 7)
ρ = air density, kg-sec^2/m^4
σ = whole number, Eqs. (25–28)
$\phi_{(x)}$ = distribution of normalized bending mode deflection, $\phi(x)\,q(t)$
ψ = phase lag, rad or deg
ω = free-free bending frequency, rad/sec
$\omega_g = 2\pi U/L_g$ = Sinusoidal gust frequency, rad/sec, Eq. (14)

Subscripts

a = attached flow
b = body
C.G. = center of gravity
g = gust
i = numbering subscript for body station
n = numbering subscript, Eq. (17a)
L = local
s = separated flow
T = total
TE = trailing edge
u = upstream communication
∞ = undisturbed flow

Superscripts

i = induced, e.g., = separation induced normal force
$(\bar{\ })$ = denotes integrated averages
$(\hat{\ })$ = Laplace transformed function

Differential symbols

$\phi'(x)$ = $\partial\phi/\partial x$
$\dot{Y}(t)$ = $\partial Y/\partial t$; $\ddot{q}(t) = \partial^2 q/\partial t^2$
$C_{N\alpha}$ = $\partial C_N/\partial_\alpha$

Presented as Paper 71-344 at the AIAA/ASME 12th Structures, Structural Dynamics and Materials Conference, Anaheim, Calif., April 19–21, 1971; submitted April 21, 1971; revision received December 6, 1972. The results were obtained in a study made for Marshall Space Flight Center, Contract NAS 8-21459, under the direction of W. W. Clever. The authors gratefully acknowledge the assistance of N. Davis in developing the needed computer programs.

Index categories: Rocket Vehicle Gust Loading and Wind Shear; Nonsteady Aerodynamics; Aeroelasticity and Hydroelasticity.

* Senior Staff Engineer. Associate Fellow AIAA.
† Research Specialist. Member AIAA.
‡ Senior Aerodynamics Engineer.

Introduction

THE separated flow regions on the Saturn-Apollo launch vehicle generated by the tower-mounted escape rocket and interstage conical fairings can have a dominant influence on the elastic vehicle dynamics.[1,2] Because the full-scale vehicle is likely to have undergone design changes after the freeze of the model design, an aeroelastic wind-tunnel test can often not be extrapolated to full scale without an analytic theory that includes the combined effects of changed geometry, mode shape, and vehicle trajectory. Even without such post test changes, the elastic vehicle response to so called sinusoidal gusts,[3,4] which have become of more and more concern as the size of the launch vehicle has grown, could not be obtained from wind tunnel experiments, as there is no facility existing today that can produce harmonically varying cross flow simulating a sinusoidal gust.

It is, thus, clear that the elastic vehicle response to sinusoidal gusts can only be determined by theoretical means. As no

pure theory exists that will predict the loads in the large regions of separated flow existing on the Apollo-Saturn launch vehicles,[2] a combined theoretical-experimental approach has to be used. The static load distribution is obtained from standard type wind-tunnel tests. It is used as an input in an analysis, which provides the needed theoretical means for prediction of the gust penetration loads and elastic vehicle response.

Realistic predictions of gust penetration loads and associated elastic vehicle response for Apollo-Saturn launch vehicles have not been provided by existing theories because of the neglect of the following effects: 1) separated flow effects on (static) aerodynamics loads, and 2) separated flow induced convective time lag effects on gust penetration loads and aerodynamic damping.

Analysis

The usual linearization approach is used, i.e., the environment is assumed to change slowly such that the time varying coefficients in the equations of motion can be represented by constant coefficients for finite time intervals in the trajectory. When the full coupled equations of motion are considered, this procedure may not always be justified, and the nonlinear equations have to be solved, either by direct numerical techniques[5]§ or by the faster method using perturbation from a reference trajectory.[6,7] Especially when rigid body gust loads are considered, the coupling with the control system must be accounted for if meaningful results are to be obtained.[8]

However, the present analysis is not intended to provide design information for the control system but rather to develop means to assess the effects of gust loads on the structural integrity of the elastic vehicle. Consequently, the gust response can be determined by superposition.[5] That is, only the linear analysis of one-degree-of-freedom bending response to gust loads will be discussed.

The aerodynamic loads in regions of attached flow are determined by combining first-order momentum theory[9] with quasi-steady instantaneous load estimates[10,11] representing the cruciform fins by an equivalent cross-sectional area distribution.[10,12]

The local loads in separated flow regions are represented in a similar manner by an effective cross-sectional area.[13,14] The separation-induced loads are extracted from static experimental data and converted into dynamic loads using quasi-steady techniques that account for the effects of convective time lag[2,10,13,15] and accelerated flow.[16,17,18]

The transverse gust velocity W_g and the vehicle velocity U are assumed to change negligibly during a time interval large enough to define the gust penetration load, e.g., the time interval required for the vehicle to travel one body length. Thus, W_g is a function of the inertial space coordinate X only.

Elastic Vehicle Response

The equation of motion for single-degree-of-freedom bending oscillations can be written in the following form using standard notations

$$\tilde{m}[\ddot{q}(t) + 2\zeta\omega\dot{q}(t) + \omega^2 q(t)] = P(t) \tag{1}$$

The generalized force $P(t)$ is given by the virtual work done by the aerodynamic forces (and axial force moments) on the vehicle.

$$P(t) = \int \frac{dN}{dx}\phi(x)dx + \int \frac{dM_A}{dx}\phi'(x)dx \tag{2}$$

§ Only one mode at a time can be at resonance, and the off-resonance response of other modes can be superimposed in the linear small perturbation analysis.

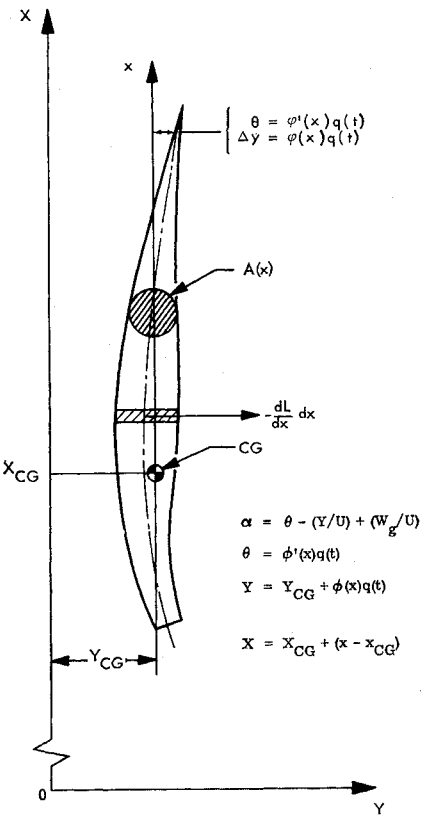

Fig. 1 Elastic body coordinate system for one-degree-of-freedom analysis.

The integrals are evaluated through summation of a discrete number of lumped forces (and axial force moments).

How the generalized force $P(t)$ is computed is shown in Ref. 19. In attached flow regions (Fig. 1), the generalized force is

$$\begin{aligned} P_a(t)\Big/\left(\frac{\rho U^2}{2}\right)S &= \int_{x_l}^{x_{l+1}} \frac{dC_N}{dx}\phi(x)dx \\ &= -\int_{x_l}^{x_{l+1}} \frac{2A(x)}{S}\phi(x)\left[\phi'(x)q(t) - \phi(x)\frac{\dot{q}(t)}{U}\right] + \\ &\int_{x_l}^{x_{l+1}} \frac{2A(x)}{S}\left\{[\phi'(x)]^2 q(t) - [\phi(x)]^2\frac{\ddot{q}(t)}{U^2}\right\}dx - \\ &\int_{x_l}^{x_{l+1}} \frac{2A'(x)}{S}\phi(x)\frac{W_g(X_{CG}+x)}{U}dx \end{aligned} \tag{3}$$

where the following slender body derivatives are readily identified

$$C_{N_\alpha}(x) = 2A(x)/S; \quad dC_{N_\alpha}(x)/dx = 2A'(x)/S \tag{4}$$

For the long wavelength gusts and lower bending modes considered in the present analysis, the area change $A'(x)$ at interstage frustums and on the command module of the Apollo-Saturn launch vehicle takes place over an x-extent that is small compared to gust and bending mode "wavelengths." Thus, in the evaluation of the integrals in Eq. (3), the x-step can be increased appreciably if the fast area change $A'(x)$ is "integrated out," considering $\phi(x)$, $\phi'(x)$, and W_g $(X_{C.G.} + x)$ constant over the x-interval between x_l and x_{l+1}.

For constant area sections the gust shear $W'_g(X)$ and the modal slope $\phi'(x)$ can be assumed to remain constant for the (small) x-interval $x_l \leq x \leq x_{l+1}$.

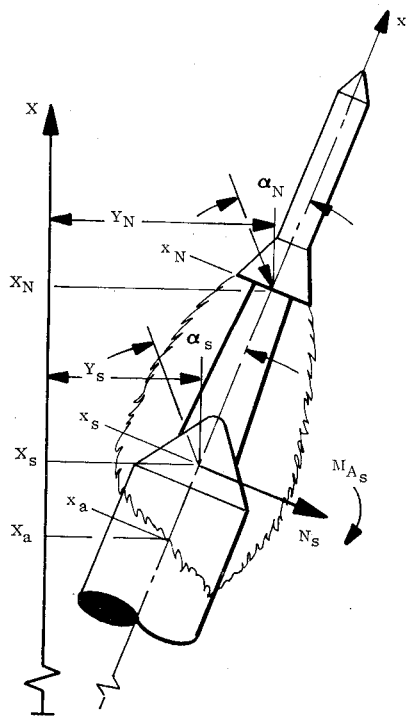

Fig. 2 Definition of separated flow parameters.

In regions of separated flow $P(t)$ is as follows (Fig. 2):

$$P_s(x_s,t) = N_s(t)\phi(x_s) + M_{A_s}(t)\phi'(x_s)$$

$$N_s(t)\Big/\left(\frac{\rho U^2}{2}\right)S = \frac{\partial C_{N_s}}{\partial \alpha_s}\left[\phi'(x_s)q(t) - \phi(x_s)\frac{\dot{q}(t)}{U}\right] +$$

$$\frac{\partial C_{N_s}}{\partial \theta_N}\phi'(x_N)q(t-\Delta t) + \frac{\partial C_{N_s}}{\partial(\dot{Y}_N/U)}\phi(x_N)\frac{\dot{q}(t-\Delta t)}{U} +$$

$$\frac{\partial C_{N_s}}{\partial y}[\phi(x_N)q(t-\Delta t) - \phi(x_s)q(t)] + \frac{\partial C_{N_s}}{\partial \alpha_s}\frac{W_g(Ut-[x_0-x_s])}{U} +$$

$$\left[(x_N - x_s)\frac{\partial C_{N_s}}{\partial y} + \frac{\partial C_{N_s}}{\partial \alpha_N}\right]\frac{W_g(Ut-[x_0-x_s]\kappa)}{U}$$

$$\kappa = 1 + \left(\frac{U}{\bar{U}} - 1\right)(x_{N_l} - x_{s_l})/(x_0 - x_{s_l}) \qquad (5)$$

$M_{A_s}t/(\rho U^2/2)Sc$ is the axial force moment term corresponding to $N_s(t)$ given by the same equation with C_{m_A} substituted for C_N). In comparing Eq. (5) with Eq. (3), one notes that the separated flow region is treated as a dead air region; that is, no body steering effects are considered. It was shown in Refs. 13 and 14 that if one included some steering effect by equating the local lift generation to that of an equivalent attached flow region with reduced cross-sectional area, improved predictions of the unsteady aerodynamics resulted.

The effective cross-sectional area in separated flow regions is determined by the average reduction in dynamic pressure, which for a flared section is given by the axial force deficit. If we assume that the density changes negligibly throughout the separated flow region, which should be permissible at the subsonic and transonic vehicle speeds of interest, the effective area is related to the mean convection velocity $\bar{U}$ as follows:

$$\bar{A}(x_l)/A(x_l) = [\bar{U}(x_l)/U(x_l)]^2 = (C_{A_F})_s/(C_{A_F})_a \qquad (6)$$

Applying this equivalent area rule gives the following expression for the generalized forces, combining Eqs. (3, 5, and 6)

$$P(t) = \sum_{l=1}^{N} P_{N_l}(t) + P_{N_{\text{Fins}}}(t) + \sum_{l=1}^{M} P_{M_l}(t)$$

$$P_{N_l}(t)\Big/\left(\frac{\rho U^2}{2}\right)S = \Bigg\{C_{N(\alpha_L)}\phi(x_{i_L})\phi'(x_{i_L}) +$$

$$\left(\frac{\bar{U}}{U}\right)^2\frac{2A(x_{l+1})}{S}[\phi(x_l)\phi'(x_l) - \phi(x_{l+1})\phi'(x_{l+1})]\Bigg\}q(t) -$$

$$\Bigg(C_{N(\alpha_L)}[\phi(x_{i_L})]^2 - \left(\frac{\bar{U}}{U}\right)^2\frac{2A(x_{l+1})}{S}\Big\{[\phi(x_l)]^2 -$$

$$[\phi(x_{l+1})]^2\Big\}\Bigg)\frac{\dot{q}(t)}{U} + \frac{2\pi}{S}\left(\frac{\bar{U}}{U}\right)^2 \times$$

$$\frac{(x_{l+1}-x_l)}{3}\left[\frac{[r(x_{l+1})]^3 - [r(x_l)]^3}{r(x_{l+1}) - r(x_l)}\right]^{\P}[\phi'(\bar{x}_l)]^2 q(t) +$$

$$C_{N(\alpha_L)}\phi(x_{i_L})\frac{W_g(Ut-[x_0-x_{i_L}])}{U} +$$

$$\left(\frac{\bar{U}}{U}\right)^2\left(\frac{2A(x_{l+1})}{S} - \frac{2A(x_l)}{S}\right)\phi(\bar{x}_l)\frac{W_g(Ut-[x_0-\bar{x}_l])}{U} +$$

$$\frac{\partial[C_{N_s}(\bar{x}_l)]}{\partial[\theta(x_{N_l})]}\phi(\bar{x}_l)\phi'(x_{N_l})\,q(t-\Delta t) +$$

$$\frac{\partial[C_{N_s}(\bar{x}_l)]}{\partial[\dot{Y}(x_{N_l})/U]}\phi(\bar{x}_l)\phi(x_{N_l})\frac{\dot{q}(t-\Delta t)}{U} +$$

$$\frac{\partial[C_{N_s}(\bar{x}_l)]}{\partial\beta}\frac{\phi(\bar{x}_l)\phi(x_{N_l})}{(\bar{x}_{N_l}-\bar{x}_l)}q(t-\Delta t) - \frac{\partial[C_{N_s}(\bar{x}_l)]}{\partial\beta}\frac{[\phi(\bar{x}_l)]^2}{(x_{N_l}-\bar{x}_l)}q(t) +$$

$$\left\{\frac{\partial[C_{N_s}(\bar{x}_l)]}{\partial[\theta(x_{N_l})]} + \frac{\partial[C_{N_s}(\bar{x}_l)]}{\partial\beta}\right\}\phi(\bar{x}_l)\frac{W_g(Ut-[x_0-\bar{x}_l]\kappa)}{U}$$

$$P_{N_{\text{Fins}}}(t)\Big/\left(\frac{\rho U^2}{2}\right)S = C_{N(\alpha_{\text{Fins}})}\Big\{\phi(x_{TE})\phi'(x_{TE})q(t) -$$

$$[\phi(x_{TE})]^2\frac{\dot{q}(t)}{U} + \phi(x_{TE})\frac{W_g(Ut-[x_0-x_{TE}])}{U}\Big\}^{**}$$

$$P_{M_l}(t)\Big/\left(\frac{\rho U^2}{2}\right)Sc = C_{m(A_{\alpha,L})}[\phi'(\bar{x}_l)]^2 q(t) -$$

$$C_{m(A_{\alpha,L})}\phi(\bar{x}_l)\phi'(\bar{x}_l)\frac{\dot{q}(t)}{U} +$$

$$\frac{\partial[C_{m(A_s)}(\bar{x}_l)]}{\partial[\theta(x_{N_l})]}\phi'(\bar{x}_l)\phi'(x_{N_l})\dot{q}(t-\Delta t) +$$

$$\frac{\partial[C_{m(A_s)}(\bar{x}_l)]}{\partial[\dot{Y}(x_{N_l})/U]}\phi'(\bar{x}_l)\phi(x_{N_l})\frac{\dot{q}(t-\Delta t)}{U} +$$

$$\frac{\partial[C_{m(A_s)}(\bar{x}_l)]}{\partial\beta}\frac{\phi'(\bar{x}_l)\phi(x_{N_l})}{(x_{N_l}-\bar{x}_l)}q(t-\Delta t) -$$

$$\frac{\partial[C_{m(A_s)}(\bar{x}_l)]}{\partial\beta}\frac{\phi'(\bar{x}_l)\phi(\bar{x}_l)}{(x_{N_l}-\bar{x}_l)}q(t) +$$

$$\left\{\frac{\partial[C_{m(A_s)}(\bar{x}_l)]}{\partial[\theta(x_{N_l})]} + \frac{\partial[C_{m(A_s)}(\bar{x}_l)]}{\partial\beta}\right\}\phi'(\bar{x}_l)\frac{W_g(Ut-[x_0-x_l]\kappa)}{U} \qquad (7)$$

¶ Equal to zero for constant area sections.

** The body portion "inside" the fins is treated as part of $\Sigma_{l=1}^{N} P_{N_l}(t)$.

$C_{N(\alpha_L)}$ is the local force derivative, i.e., $C_{N(\alpha_L)} = \partial C_{N_s}/\partial\alpha_s$ at $x_{i_L} = \bar{x}_i$ in separated flow regions and equal to the total normal force derivative over an area changing section ending at $x_{i_L} = x_i$ in attached flow regions

($C_{m(A_\alpha, L)}$ is always the separated flow derivative $\partial C_{m_A}/\partial\alpha_s$)

As the structural stiffness is an order of magnitude larger than the aerodynamic stiffness, the effect of aerodynamic forces on the bending frequency is negligibly small. The structural and aerodynamic damping are two orders of magnitude less than critical. Consequently, the vehicle may be assumed to describe harmonic oscillations with the natural free-free bending frequency, and $q(t-\Delta t)$ can be expressed as follows:

$$q(t-\Delta t) = e^{-i\omega\Delta t}q(t) = \cos(\omega\Delta t)q(t) - \sin(\omega\Delta t)[iq(t)]$$

where

$$\dot{q}(t) = \omega[iq(t)]\dagger\dagger \tag{8}$$

Using Eq. (8), simplified for the slow frequencies of practical interest in the present quasi-steady analysis, i.e., with cos $\omega\Delta t = 1$ and $\sin\omega\Delta t = \omega\Delta t$, gives Eq. (7) in the following form:

$$P(t) = \frac{\rho U^2}{2} S\left\{\left(\sum_{i=1}^{N} K_i + K_{\text{Fins}}\right)q(t) + \left(\sum_{i=1}^{N} D_i + D_{\text{Fins}}\right)\frac{\dot{q}(t)}{U} + \sum_{i=1}^{N} G_i(t) + G_{\text{Fins}}(t)\right\}$$

$$K_i = C_{N(\alpha_L)}\phi(x_{i_L})\phi'(x_{i_L}) + cC_{m(A_{\alpha,L})}[\phi'(\bar{x}_i)]^2 +$$

$$\left(\frac{\bar{U}}{U}\right)^2 \frac{2A(x_{i+1})}{S}[\phi(x_i)\phi'(x_i) - \phi(x_{i+1})\phi'(x_{i+1})] + \frac{2\pi}{S}\left(\frac{\bar{U}}{U}\right)^2 \times$$

$$\left(\frac{x_{i+1}-x_i}{3}\right)\left(\frac{[r(x_{i+1})]^3 - [r(x_i)]^3}{r(x_{i+1}) - r(x_i)}\right)\ddagger\ddagger [\phi'(\bar{x}_i)]^2 +$$

$$\left\{\frac{\partial[C_{N_s}(\bar{x}_i)]}{\partial[\theta(x_{N_i})]}\phi(\bar{x}_i) + \frac{\partial[C_{m(A_s)}(\bar{x}_i)]}{\partial[\theta(x_{N_i})]}c\phi'(x_i)\right\}\phi'(x_{N_i}) +$$

$$\left\{\frac{\partial[C_{N_s}(\bar{x}_i)]}{\partial\beta}\phi(\bar{x}_i) + \frac{\partial[C_{MA_s}(\bar{x}_i)]}{\partial\beta}c\phi'(\bar{x}_i)\right\}\frac{\phi(x_{N_i}) - \phi(\bar{x}_i)}{(x_{N_i} - \bar{x}_i)}$$

$$K_{\text{Fins}} = C_{N(\alpha_{\text{Fins}})}\phi(x_{TE})\phi'(x_{TE})$$

$$D_i = -C_{N(\alpha_L)}[\phi(x_{i_L})]^2 -$$

$$cC_{m(A_{\alpha,s})}\phi(\bar{x}_i)\phi(x_i)\phi'(\bar{x}_i) -$$

$$\left(\frac{\bar{U}}{U}\right)^2 \frac{2A(x_{i+1})}{S}\{[\phi(x_i)]^2 - [\phi(x_{i+1})]^2\} - \left\{\frac{\partial[C_{N_s}(\bar{x}_i)]}{\partial[\theta(x_{N_i})]}\phi(\bar{x}_i) + \frac{\partial[C_{m(A_s)}(\bar{x}_i)]}{\partial[\theta(x_{N_i})]}c\phi'(\bar{x}_i)\right\}\phi'(x_{N_i})U\Delta t_i - \left\{\frac{\partial[C_{N_s}(x_i)]}{\partial[\dot{Y}(x_{N_i})/U]}\phi(\bar{x}_i) + \frac{\partial[C_{m(A_s)}(x_i)]}{\partial[\dot{Y}(x_{N_i})/U]}c\phi'(\bar{x}_i)\right\}\phi(x_{N_i}) - \left\{\frac{\partial[C_{N_s}(\bar{x}_i)]}{\partial\beta}\phi(\bar{x}_i) + \frac{\partial[C_{m(A_s)}(\bar{x}_i)}{\partial\beta}c\phi'(\bar{x}_i)\right\}\frac{\phi(x_{N_i})U\Delta t_i}{(x_{N_i} - \bar{x}_i)}$$

$$D_{\text{Fins}} = -C_{N(\alpha_{\text{Fins}})}[\phi(c_{TE})]^2$$

$$G_i(t) = C_{N(\alpha_L)}\phi(x_{i_L})\frac{W_g(Ut - [x_0 - x_{i_L}])}{U} +$$

$$cC_{m(A_{\alpha,s})}\phi'(\bar{x}_i)\frac{W_g(Ut - [x_0 - \bar{x}_i])}{U} +$$

$$\left(\frac{\bar{U}}{U}\right)^2\left[\frac{2A(x_{i+1})}{S} - \frac{2A(x_i)}{S}\right]\phi(\bar{x}_i)\frac{W_g(Ut - [x_0 - \bar{x}_i])}{U} +$$

$$\left\{\frac{\partial[C_{N_s}(\bar{x}_i)]}{\partial[\theta(x_{N_i})]} + \frac{\partial[C_{N_s}(\bar{x}_i)]}{\partial\beta}\right\}\phi(\bar{x}_i)\frac{W_g(Ut - [x_0 - \bar{x}_i]\kappa)}{U} +$$

$$\left\{\frac{\partial[C_{m(A_s)}(\bar{x}_i)]}{\partial[\theta(x_{N_i})]} + \frac{\partial C_{m(A_s)}(\bar{x}_i)]}{\partial\beta}\right\}c\phi'(x_i)\frac{W_g(Ut - [x_0 - \bar{x}_i]\kappa)}{U}$$

$$G_{\text{Fins}}(t) = C_{N(\alpha\text{Fins})}\phi(x_{TE})\frac{W_g(Ut - [x_0 - x_{TE}])}{U} \tag{9}$$

The time-lag effect is usually obtained as follows:

$$U\Delta t_i = (x_{N_i} - \bar{x}_i)\Big/\left(\frac{\bar{U}}{U}\right) \tag{10}$$

In regions of shock-induced separation upstream of interstage flares, x_{N_i} is substituted by x_{A_C}, the aerodynamic center for the loads on the body upstream of the separation. This is true for the separation-induced negative cylinder load. For the positive load induced on the flare, an additional time lag through the separated flow region is realized. A detailed description of these deviations is given in Ref. 10.

It has been demonstrated that, in addition to the downstream convection effect on bodies submerged in wakes, upstream communication effects will in some cases become important.[13-16] The modification needed to include these upstream communication effects in the computation has been described in Refs. 13 and 14. The results of a recently completed study[16] indicate that the upstream communication effects are negligible except for certain critical geometries.

By combining Eqs. (1) and (9), the equation of motion for single-degree-of-freedom bending oscillations can be written in the following form

$$\ddot{q}(t) + 2\omega\left[\zeta - \frac{B}{2\omega U}\left(\sum_{i=1}^{N} D_i + D_{\text{Fins}}\right)\right]\dot{q}(t) + \omega^2\left[1 - \frac{B}{\omega^2}\left(\sum_{i=1}^{N} K_i + K_{\text{Fins}}\right)\right]q(t) = B\left[\sum_{i=1}^{N} G(t) + G_{\text{Fins}}(t)\right] \tag{11}$$

Since the aerodynamic stiffness is negligible compared to the structural stiffness, Eq. (11) can be approximated as

$$\ddot{q}(t) + 2\omega\zeta_T\dot{q}(t) + \omega^2 q(t) = g(t)$$

$$\zeta_T = \zeta - \frac{B}{2\omega U}\left(\sum_{i=1}^{N} D_i + D_{\text{Fins}}\right)$$

$$g(t) = B\left[\sum_{i=1}^{N} G_i(t) + G_{\text{Fins}}(t)\right] \tag{12}$$

where

$$\left(\sum_{i=1}^{N} D_i + D_{\text{Fins}}\right)$$

is given by Eq. (9).

†† This makes $2\zeta\omega\dot{q}(t)$ in Eq. (1) equivalent to the often used notation $ig\omega^2 q(t)$, where $g = 2\zeta$.

‡‡ Equal to zero for constant area sections.

The gust function $g(t)$ is defined through Eq. (9) as follows (using time rather than the space coordinate X as independent variable):

$$g(t) = \sum_{i=1}^{N_1} C_{1_i} \frac{W_g(t-[x_0-x_i]/U)}{U} + \sum_{i=1}^{N_2} C_{2_i} \frac{W_g(t-[x_0-\bar{x}_i]/U)}{U} + \sum_{i=1}^{N_3} C_{3_i} \frac{W_g(t-[x_0-\bar{x}_i]\kappa/U)}{U} + BC_{N(\alpha\text{Fins})}\phi(x_{TE}) \frac{W_g(t-[x_0-x_{TE}]/U)}{U}$$

$$C_{1_i} = BC_{N(\alpha L)}\phi(x_i)$$

$$C_{2_i} = B\left\{C_{N(\alpha_s)}\phi(\bar{x}_i) + cC_{m(A\alpha,s)}\phi'\bar{x}_i) + \left(\frac{\bar{U}}{U}\right)^2\left[\frac{2A(x_{i+1})}{S} - \frac{2A(x_i)}{S}\right]\right\}$$

$$C_{3_i} = B\left\{\frac{\partial[C_{N_s}(\bar{x}_i)]}{\partial[\theta(x_{N_i})]} + \frac{\partial[C_{N_s}(\bar{x}_i)]}{\partial\beta}\right\}\phi(\bar{x}_i) + B\left\{\frac{\partial[C_{m(A_s)}(\bar{x}_i)]}{\partial[\theta(x_{N_i})]} + \frac{\partial[C_{m(A_s)}(\bar{x}_i)]}{\partial\beta}\right\}c\phi'(\bar{x}_i) \quad (13)$$

The sinusoidal gust is defined as follows:

$$\frac{\overline{W}_g[t-(x_0-x)/U]}{U}\Big/\frac{\Delta W_g}{U} = \sin\left(\omega_g\left[t-\frac{x_0-x}{U}\right]\right) \quad (14)$$

Using Laplace transformation, Eq. (13) can be written in the frequency domain in the following form (see, for example, Ref. 20):§§

$$\hat{q}(s) = \hat{q}_0(s) + \hat{q}_g(s)$$

$$\hat{q}_0(s) = [\dot{q}(0) + (s+2\omega\zeta_T)q(0)]/D(s)$$

$$\hat{q}_g(s) = \hat{\bar{g}}(s)/D(s);\ D(s) = s^2 + 2\omega\zeta_T s + \omega^2 \quad (15)$$

$q(0)$ and $\dot{q}(0)$ are the normalized bending mode deflection and deflection rate at gust entry, respectively. The Laplace transform of Eq. (13) gives the following definition of $\hat{q}_{\bar{g}}(s)$:

$$\hat{q}_{\bar{g}}(s) = \hat{f}(s)\left\{\sum_{i=1}^{N_1} C_{1_i}\exp\left[-\left(\frac{x_0-x_i}{U}\right)s\right] + \sum_{i=1}^{N_2} C_{2_i}\exp\left[-\left(\frac{x_0-\bar{x}_i}{U}\right)s\right] + \sum_{i=1}^{N_3} C_{3_i}\exp\left[-\left(\frac{x_0-\bar{x}_i)\kappa}{U}\right)s\right] + BC_{N(\alpha\text{Fins})}\phi x_{TE})\exp\left[-\left(\frac{x_0-x_{TE}}{U}\right)s\right]\right\} \hat{f}(s) = \frac{\hat{\overline{W}}_g(s)}{U}\Big/D(s) \quad (16)$$

The corresponding formulation in the time domain can be written[20]

$$q\hat{\bar{g}}(t) = \sum_{i=1}^{N_1} C_{1_i} f\left(t-\frac{x_0-x_i}{U}\right) + \sum_{i=1}^{N_2} C_{2_i} f\left(t-\frac{x_0-\bar{x}_i}{U}\right) + \sum_{i=1}^{N_3} C_{3_i} f\left(t-\frac{[x_0-\bar{x}_i]\kappa}{U}\right) + BC_{N(\alpha\text{Fins})}\phi(x_{TE}) f\left(t-\frac{x_0-x_{TE}}{U}\right) \quad (17)$$

§§ The transformation pair No. 1.359 of Ref. 21, pertaining to this exact situation, is unfortunately incorrect; and the formulations in AIAA paper 71-344 are, as a consequence, also incorrect.

For the gust profile given by Eq. (11), the following expression is obtained for for $\hat{f}(s)$ and $f(t)$ (Ref. 20).

$$\hat{f}(s)\Big/\frac{\Delta W_g}{U} = \omega_g/(s^2+\omega_g^2)D(s) \quad (18)$$

$$f(t) = \frac{\Delta W_g}{U}\left\{\sin(\omega_g t - \psi_1) + \frac{\exp(-\omega\zeta_T t)}{(\sin\psi_2/\sin\psi_1)}\sin(\omega t[1-\zeta_T{}^2]^{1/2} - \psi_2)\right\}/\omega_g{}^2\{[(\omega/\omega_g)^2-1]^2 + 4(\omega/\omega_g)^2\zeta_T{}^2\}^{1/2}$$

$$\tan\psi_1 = \frac{2(\omega/\omega_g)\zeta_T}{(\omega/\omega_g)^2-1};\ \tan\psi_2 = -\frac{2(\omega/\omega_g)^2\zeta_T(1-\zeta_T{}^2)^{1/2}}{(\omega/\omega_g)^2(1-2\zeta_T{}^2)-1} \quad (19)$$

As $\zeta_T{}^2 \ll 1$ Eq. (19) can be simplified as follows:

$$f(t) = \frac{\Delta W_g}{U} \times \frac{\sin(\omega_g t - \psi_1) + (\sin\psi_1/\sin\psi_2)\exp(-\omega\zeta_T t)\sin(\omega t - \psi_2)}{\omega^2\{[1-(\omega_g/\omega)^2]^2 + 4(\omega_g/\omega)^2\zeta_T{}^2\}^{1/2}} \times$$

$$\tan\psi_1 = \frac{2(\omega_g/\omega)\zeta_T}{1-(\omega_g/\omega)^2};\ \tan\psi_2 = -\frac{2\zeta_T}{1-(\omega_g/\omega)^2} \quad (20)$$

or

$$f(t) = -\frac{\Delta W_g}{U}\frac{1}{\omega^2}\frac{1}{2\zeta_T}\frac{1-\exp(-\omega\zeta_T t)}{[1+(\varepsilon/\zeta_T)^2]^{1/2}}\cos\left(\omega t + \arctan\frac{\varepsilon}{\zeta_T}\right)$$

where

$$\omega/\omega_g = 1+\varepsilon;\ |\varepsilon| \ll 1;\ \xi_T \neq 0 \quad (21)$$

The effect of the initial conditions at gust entry can be expressed as follows:[20]

$$\Delta q_0(t') = \Delta q_0\exp(-\omega\zeta_T t')\cos(\omega t' + \psi_0)$$

$$\Delta q_0 = q(0)(1+[2\zeta_T = \dot{q}(0)/\omega q(0)])^{1/2}\exp(-\omega\zeta_T\Delta t_0) \quad (22)$$

$$\psi_0 = \omega\Delta t_0 - \arctan[\zeta_T + \dot{q}(0)/\omega q(0)]$$

$$t = t' + \Delta t_0$$

That is, the initial conditions can be expresssed by the amplitude Δq_0 and phase angle ψ_0 at gust entry. For the linear analysis performed here, the effects of these oscillatory parameters at gust entry on the over-all bending response can be superimposed on the gust response.

Combining Eq. (17) with Eqs. (20) and (21) gives the following definitions of the bending response to sinusoidal gusts. For algebraic shorthand purposes, Eq. (17) is represented by the following formulation:

$$q_{\bar{g}}(t) = \sum_{n=1}^{N} C_n f(t-\Delta t_n) \quad (17a)$$

$$\omega_g \neq \omega$$

$$q_{\bar{g}}(t) = \left\{\frac{\Delta W_g}{U}\Big/\omega^2\{[1-\omega_g/\omega)^2]^2 + 4(\omega_g/\omega)^2\zeta_T{}^2\}^{1/2}\right\} \times \left\{(E_1{}^2+E_2{}^2)^{1/2}\sin\left(\omega_g t - \arctan\frac{E_2}{E_1}\right) + (\sin\psi_1/\sin\psi_2)\exp(-\omega\zeta_T t)(E_3{}^2+E_4{}^2)^{1/2}\sin\left(\omega t - \arctan\frac{E_4}{E_3}\right)\right\}$$

$$E_1 = \sum_{n=1}^{N} C_n\cos\psi_{1_n};\ E_2 = \sum_{n=1}^{N} C_n\sin\psi_{1_n}$$

$$E_3 = \sum_{n=1}^{N} C_n \exp(\omega\zeta_T \Delta t_n)\cos\psi_{2n};\quad E_4 = \sum_{n=1}^{N} C_n \exp(\omega\zeta_T \Delta t_n)\sin\psi_{2n}$$

$$\tan\psi_1 = \frac{2(\omega_g/\omega)\zeta_T}{1-(\omega_g/\omega)^2};\quad \tan\psi_2 = -\frac{2\zeta_T}{1-(\omega_g/\omega)^2}$$

$$\psi_{1n} = \psi_1 + \omega_g \Delta t_n;\quad \psi_{2n} = \psi_2 + \omega\Delta t_n \qquad (23)$$

$$(\omega/\omega_g) = 1 + \varepsilon;\quad |\varepsilon| \ll 1;\quad \zeta_T \neq 0$$

$$q_{\bar{g}}(t) = \left\{\frac{\Delta W_g}{U}\Big/ 2\omega^2\zeta_T\{1+(\varepsilon/\zeta_T)^2\}^{1/2}\right\} \times$$

$$\left\{(F_1^2+F_2^2)^{1/2}\cos\left(\omega t - \arctan\frac{F_2}{F_1}\right) - \right.$$

$$\left. \exp(-\omega\zeta_T t)(F_3^2+F_4^2)^{1/2}\cos\left(\omega t - \arctan\frac{F_4}{F_3}\right)\right\}$$

$$F_1 = \sum_{n=1}^{N} C_n\cos\Delta\psi_n;\quad F_2 = \sum_{n=1}^{N} C_n\sin\Delta\psi_n$$

$$F_3 = \sum_{n=1}^{N} C_n \exp(\omega\zeta_T\Delta t_n)\cos\Delta\psi_n;\quad F_4 =$$

$$\sum_{n=1}^{N} C_n \exp(\omega\zeta_T\Delta t_n)\sin\Delta\psi_n$$

$$\Delta\psi_n = \omega\Delta t_n - \arctan(\varepsilon/\zeta_T) \qquad (24)$$

Only a small number (ν) of consecutive sinusoidal gust waves are realized in actual flight through the atmosphere. For that reason, only the early time resonant response is of practical interest. The exponential in Eq. (21) can be approximated by a series expansion. Equations (21) and (17a) give for $\epsilon = 0$, $\omega\zeta_T t < 1$ the following resonant response:

$$q_{\bar{g}}(t) = -\frac{\Delta W_g}{U}\frac{\pi}{\omega^2}\sum_{n=1}^{N} C_n[\Delta\nu - \nu_n]\cos\zeta\pi(\nu - \Delta\nu_n) \qquad (25)$$

$$\{1 - [\pi\zeta_T(\nu - \Delta\nu_n)] + \tfrac{2}{3}[\pi\zeta_T(\nu - \Delta_n)]^2 \ldots\}$$

$$\Delta\nu_n = \kappa_n[(x_0 - x_n)/L_b]L_b/L_g$$

Thus, the damping ζ_T has only a second order effect on the early time resonant response.

Discussion of Results

The elastic vehicle response of the Saturn V (SAS-508) as a function of penetration depth into a sinusoidal gust is shown in Fig. 3. The gust-induced bending moment¶¶ reaches its maximum (steady-state) value shortly after full penetration into the gust (Fig. 3a). The elastic vehicle response amplitude is, in contrast, still growing after 10 body lengths penetration (Fig. 3b). The variation of the maximum gust-induced bending moment with gust wavelength is shown in Fig. 4

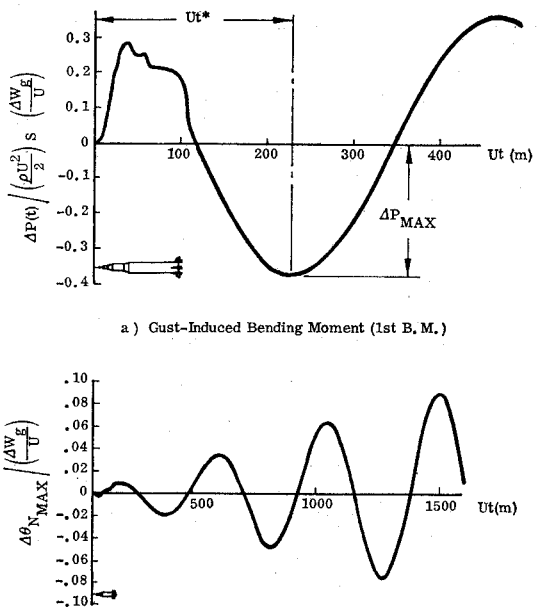

Fig. 3 Saturn V (AS-508) elastic body gust penetration effects as a function of penetration depth into sinusoidal gusts ($\omega_g/\omega = 1$) at maximum pressure ($M = 1.6$).

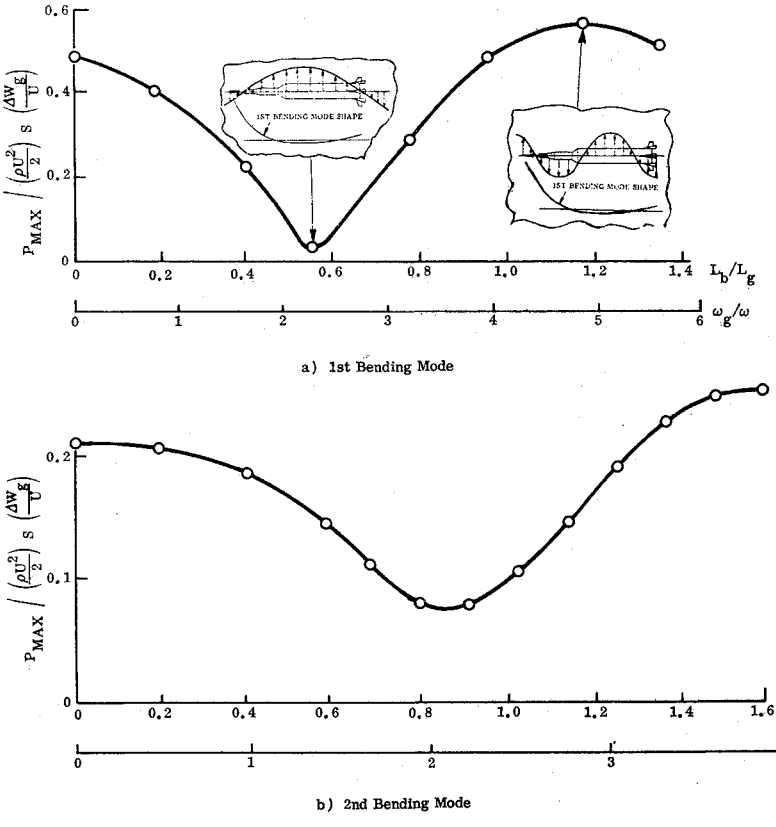

Fig. 4 Maximum gust-induced bending moment for Saturn V (AS-508) at maximum dynamic pressure ($M = 1.6$).

¶¶ The generalized force for elastic vehicle bending in one of the free-free bending modes.

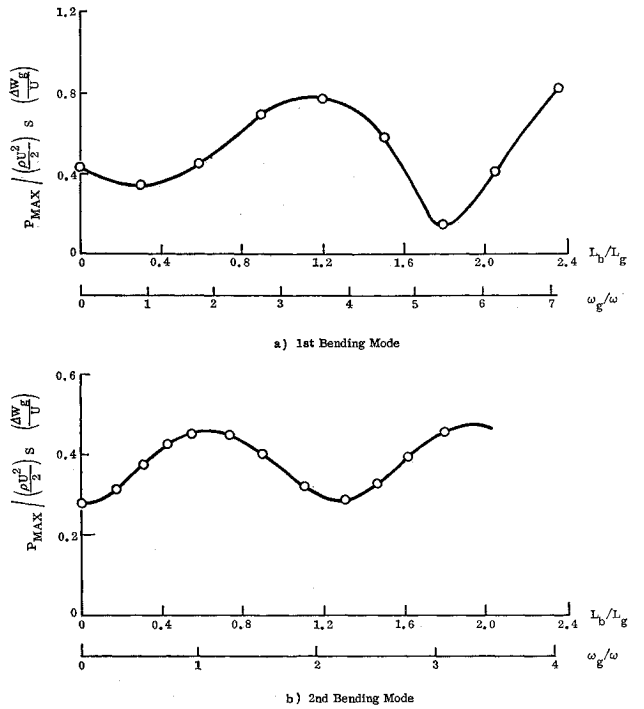

Fig. 5 Maximum gust-induced bending moment for Saturn I with disk-on escape rocket at $M = 0.9$.

for the Saturn V launch vehicle. Figure 5 shows the same for the Saturn I launch vehicle.* The launch vehicle positions in the gust wave for "peaks" and "valleys" of the maximum gust-induced bending moment are illustrated for the first bending mode of Saturn V by the insets in Fig. 4a. One notices with some concern that the gust-induced moment at resonance ($\omega_g/\omega = 1$) is near maximum for the second bending mode of Saturn I (Fig. 5b). As a consequence, the second bending mode response $\Delta\theta_{N\,max}$ is also near maximum for the Saturn I vehicle (Fig. 6b). In contrast, both the first and second bending mode response for the Saturn V vehicle are far from the maximum possible (Figs. 4 and 7). Even in this case, however, it is the resonant response that is highest and produces the critical gust design loads.†

The maximum possible response at resonance for Saturn V is substantially higher than that shown in Fig. 7. It would be reached if the structural rigidity were changed such that the gust-induced moment reached a maximum when the gust wavelength gave resonance conditions for one of the bending modes. For a simple cone-cylinder-fin geometry, the critical stiffness and associated natural body bending frequency giving maximum elastic vehicle gust response at resonance can be determined very simply, using only two lumped loads separated by a distance L_b* slightly shorter than the total body length L_b.

The maximum elastic vehicle response at resonance will occur when the characteristic body length L_b* (where $L_b^* \approx L_b$) is related to the gust wavelength L_g as follows ($\sigma = 1, 2, 3,$ etc.):

$$L_b^*/L_g = \begin{cases} \sigma & : \text{Odd No. B.M.} \\ \sigma + 1/2 & : \text{Even No. B.M.} \end{cases} \qquad (26)$$

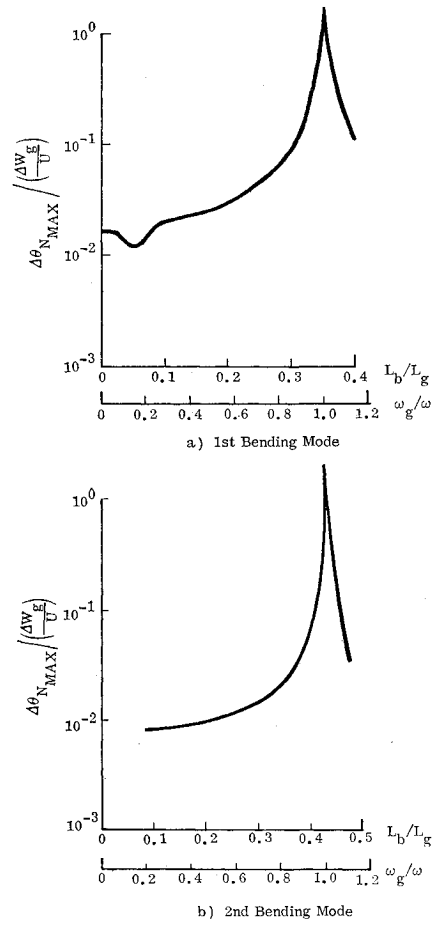

Fig. 6 Maximum elastic vehicle response at $M = 0.9$ of Saturn I with disk-on escape rocket ($\zeta = 0.01$).

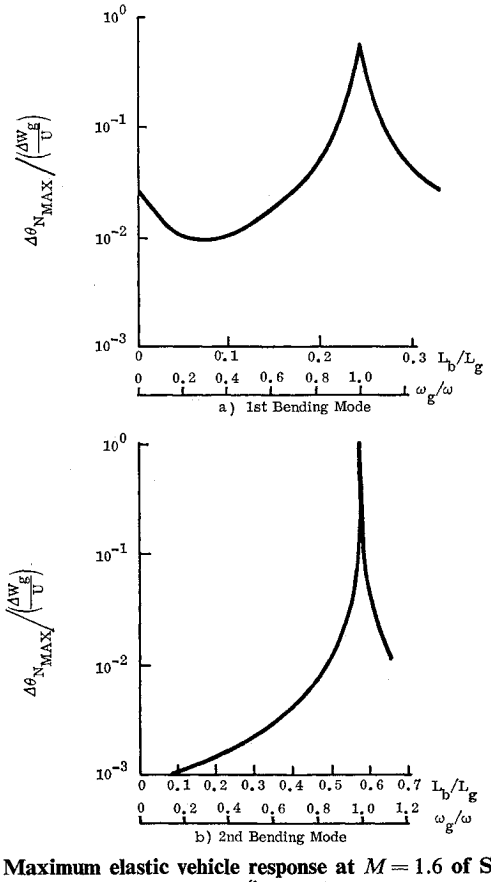

Fig. 7 Maximum elastic vehicle response at $M = 1.6$ of Saturn V (AS-508, $\zeta = 0.01$).

* Because of an error in the computer program, the results for the first mode gust-induced bending moments for Saturn V and Saturn I shown in Figs. 15–18 of Ref. 19 are not correct. The difference is small, however, and is completely without significance for the discussion of results in Ref. 19. Only when computing the response, which is done in the present paper, does the actual quantitative *P*-data become important.

† The requirement of quasi-steadiness puts upper limits of $L_b/L_g = 7$ and 4 for Saturn V and Saturn I, respectively. This makes the axial extent of the critical separated flow region, the escape rocket wake, less than one-quarter of the gust wave length.

Conversely, the minimum gust-induced response at resonance will be obtained when

$$L_b^*/L_g = \begin{cases} \sigma + 1/2: \text{ Odd No. B. M.} \\ \sigma \quad\quad : \text{Even No. B. M.} \end{cases} \tag{27}$$

Thus, a critical Strouhal number S^* giving maximum elastic vehicle response to sinusoidal gusts (at resonance) can be defined as follows:

$$S_{crit}^* = \frac{(\omega/2\pi)L_b^*}{U} = \begin{cases} \sigma \quad\quad : \text{Odd No. B.M.} \\ \sigma + 1/2: \text{Even No. B.M.} \end{cases} \tag{28}$$

It would obviously be wise to design the launch vehicle such that the structural rigidity did not generate a critical Strouhal number, especially not for any of the lower bending modes. The increasing dominance of structural damping with increasing natural bending frequency makes the higher mode shapes less prone to exhibit any large amplitude response The goal should, of course, be to get as close as possible to the optimum stiffness—that giving minimum gust response at resonance—which is given by the optimum Strouhal number defined below

$$S_{opt}^* = \frac{(\omega/2\pi)L_b^*}{U} = \begin{cases} \sigma + 1/2: \text{ Odd No. B.M.} \\ \sigma \quad\quad : \text{Even No. B. M.} \end{cases} \tag{29}$$

The simple geometry discussed above represents a great number of military missiles and civilian launch vehicles. The Apollo-Saturn launch vehicles, however, usually have more complicated geometries, and the maximum (and minimum) possible elastic vehicle response can be determined only through more involved computations. First, the wavelengths giving maximum (and minimum) gust-induced bending moments are determined, and the resonant vehicle response is then computed using the (fictitious) bending mode frequency giving resonant conditions at these critical gust wavelengths.

The data in Figs. 6 and 7 are for infinite penetration into a sinusoidal gust of unit amplitude ($\Delta W_g/U = 1$). In reality, only a limited number of consecutive sinusoidal waves will be available.[3] The measured sinusoidal gusts in the Earth's atmosphere are represented in statistical form in Fig. 8. According to those data, the AS-508 vehicle would experience the gust-induced nose amplitude shown in Fig. 9. The figure shows the maximum response, i. e., the maximum dynamic pressure data of Fig. 4 converted into real loads and deflections by use of the data in Fig. 8. Figure 10 shows

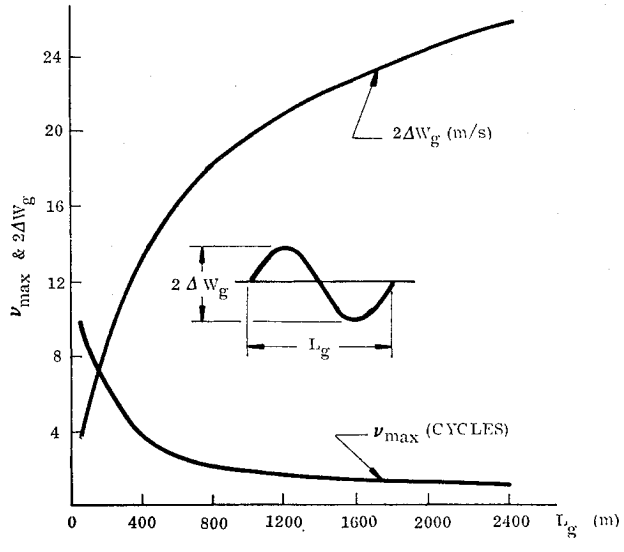

Fig. 8 Atmospheric gust amplitude and frequency data for sinusoidal gusts.[3]

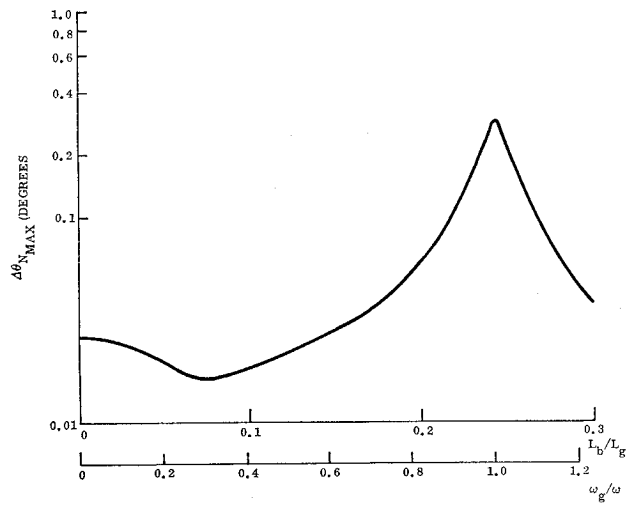

Fig. 9 Saturn V (AS-508) maximum elastic vehicle response as a function of sinusoidal gust wavelength at maximum dynamic pressure ($M = 1.6$, 1st B.M., $\zeta = 0.01$, $\nu = \nu_{max}$).

how the response at resonance after penetration of a finite number of gust cycles, $\nu \leq \nu_{max}$ of Fig. 8, is insensitive to the (structural) damping, even though the steady state response is highly sensitive to the damping. [This is also shown more directly by Eq. (25).]

In Fig. 11 the effect of gust wavelength on the Saturn I (AS-9) elastic vehicle response is shown. The agreement between present computations and Papadopoulus' results[22] is somewhat surprising since Papadopoulus assumed attached flow aerodynamics, which are very different from the measured aerodynamic loading including the effects of separated flow.[19]

The nose deflection amplitudes $\Delta\theta_{N\,max}$ shown in Fig. 9 are large, especially at resonance. In order to get some idea

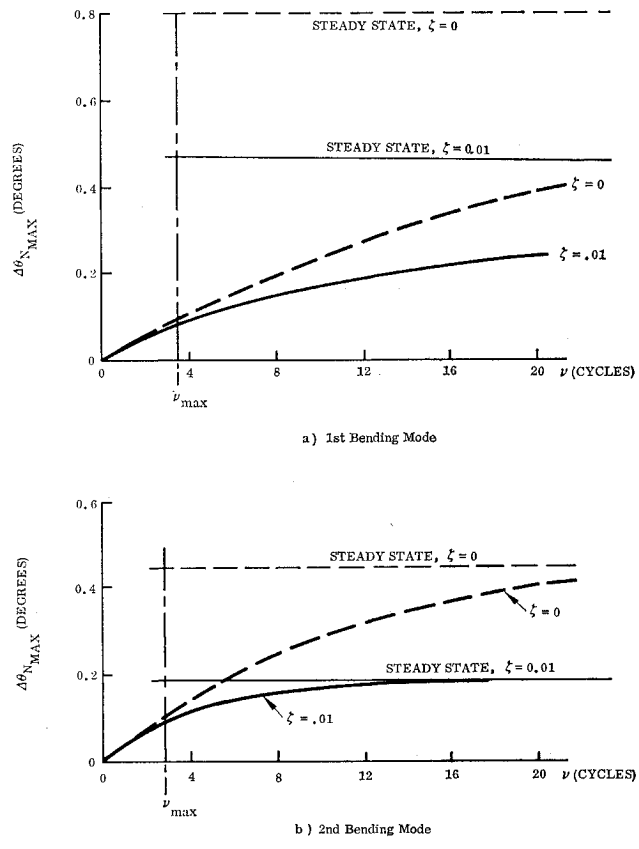

Fig. 10 Saturn I (AS-9) resonant response amplitude as a function of number of oscillation cycles.

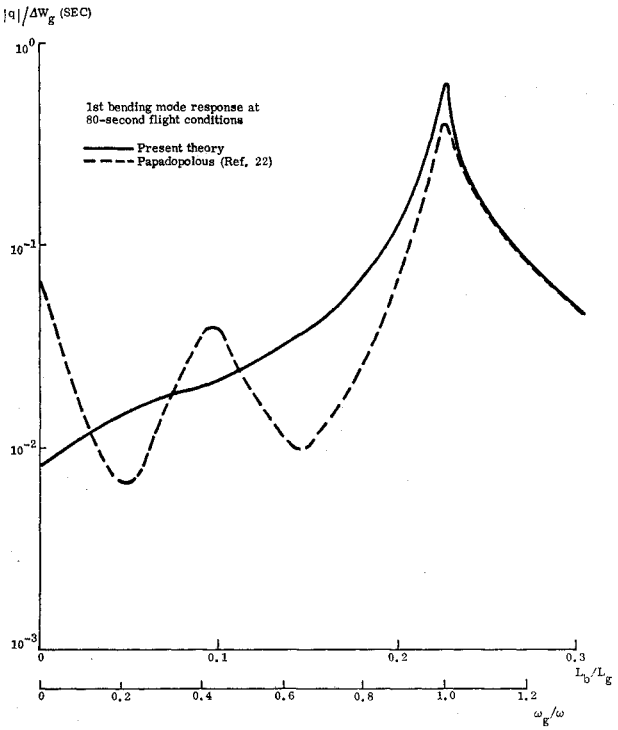

Fig. 11 Saturn I (AS-9) elastic vehicle response to sinusoidal gusts as determined by present and previous theories (1st B.M.).

about how severe they are, a simple analysis was performed to give a comparison between the stresses caused by nose amplitude $\Delta\theta_N$ and the steady state angle of attack α (Ref. 23). For the Saturn V vehicle a 1° dynamic nose amplitude ($\Delta\theta_N = 1°$) corresponds to a 10° static angle of attack ($\alpha = 10°$) in regard to the maximum stress level on the forward half of the vehicle. That is, the maximum amplitude response $\Delta\theta_N$ shown in Figs. 9 and 10 gives cause for concern, especially when combined with static loads for $\alpha \neq 0$.

Summary and Conclusions

A study of the elastic vehicle response of Apollo-Saturn launch vehicles to sinusoidal gusts has shown the following: 1) For large launch vehicles such as the Saturn boosters, long wavelength sinuoidal gusts can generate critical loads; 2) An optimum structural frequency (or structural stiffness) can be defined that will minimize the critical gust-induced design load caused by the resonant amplitude response; 3) The elastic vehicle resonant response to sinuoidal gusts could determine the critical design loads.

References

[1] Rainey, A. G., "Progress on the Launch Vehicle Buffeting Problem," *Journal of Spacecraft and Rockets*, Vol. 2, No. 3, May-June 1965, pp. 289–299.

[2] Ericsson, L. E. and Reding, J. P., "Analysis of Flow Separation Effects on the Dynamics of a Large Space Booster," *Journal of Spacecraft and Rockets*, Vol. 2, No. 4, July–Aug. 1965, pp. 481–490.

[3] Vaughn, W. W., "Sinusoidal Gust Criteria Guidline for Apollo Emergency Detection System Angular Rate Studies," Memo R-AERO-Y-31-64, June 1964, NASA.

[4] Daniel, G. E., Scogins, J. R., and Smith, O. E., "Terrestrial Environment (Climatic) Criteria Guidelines for Use in Space Vehicle Development," 1966 Revision, TM X-53328, May 1, 1966, NASA.

[5] Lester, H. C. and Morgan, H. G., "Determination of Launch Vehicle Response to Detailed Wind Profiles," *Journal of Spacecraft and Rockets*, Vol. 2, No. 1, Jan.-Feb. 1965, pp. 62–67.

[6] Ryan, R. S., Coffin, T., and Fontenot, L. L., "Dynamic Loads of a Launch Vehicle Due to Inflight Winds," *Proceedings of the 3rd National Conference on Aerospace Meteorology*, American Meteorological Society,Boston, Mass., 1968, pp. 337–345.

[7] Van Der Maas, C. J., "High-Speed Analysis of Wind-Induced Dynamic Loads on Vertically Rising Vehicles," *Journal of Spacecraft and Rockets*, Vol. 4, No. 5, May 1967, pp. 583–591.

[8] Blackburn, R. R. and St. John, A. D., *Effects and Importance of Penetration and Growth of Lift on Space Vehicle Response*, CR-326, Contract NAS 8-11012, Nov. 1965, NASA.

[9] Bisplinghoff, R. L., Ashley, H., and Halfman, R. L., *Aeroelasticity*, Addison-Wesley, Cambridge, Mass., 1965, pp. 418, 419.

[10] Ericsson, L. E. and Reding, J. P., "Report on Saturn I-Apollo Unsteady Aerodynamics," Rept. LMSC-A650215, Contract NAS 8-5338, Feb. 1964, Lockheed Missiles & Space Co. Inc., Sunnyvale, Calif.

[11] Wells, C. R. and Mitchell, H. P., "A Mathematical Model for Flexible Response of Uprated Saturn I Inflight Winds," *Journal of Spacecraft and Rockets*, Vol. 5, No. 3, March 1968, pp. 313–320.

[12] Glauz, W. D. and Blackburn, R. R., *Study of Indical Aerodynamic Forces on Multistage Space Vehicle Systems*, Vol. 1, *Application of Theory to Basic Geometries and to the Saturn V*, Final Rept., June 1962-Sept. 1968, Contract NAS 8-21167, MRI Project 3089-P, Midwestern Research Inst, Kansas City, Mo.

[13] Ericsson, L. E. and Reding, J. P., "Aeroelastic Characteristics of Saturn 1B and Saturn V Launch Vehicles," TRM-37-67-5, Contract NAS 8-11238, Dec. 1967, Lockheed Missiles & Space Co., Inc., Sunnyvale, Calif.

[14] Reding, J. P., "Partial Simulation of Elastic Body Dynamics for the Upper Stages Apollo-Saturn Launch Vehicles," LMSC Rept. M-37-67-4, Contract NAS 8-12238, Dec. 1967, Lockheed Missiles & Space Co. Inc., Sunnyvale, Calif.

[15] Ericsson, L. E. and Reding, J. P., "Dynamics of Separated Flow over Blunt Bodies," Technical Summary Rept. 2-80-65-1 Contract NAS 8-5338, Dec. 1965, Lockheed Missiles & Space Co. Inc., Sunnyvale, Calif.

[16] Ericsson, L. E., Reding, J. P., and Guenther, R. A., "Effects of Shock-Induced Separation," Technical Summary Rept. L-87-69-1, Contract NAS 8-20354, June 1969, Lockheed Missiles & Space Co. Inc., Sunnyvale, Calif.

[17] Ericsson, L. E., "Aeroelastic Instability Caused by Slender Payloads," *Journal of Spacecraft and Rockets*, Vol. 4, No. 1, Jan. 1967, pp. 65–73.

[18] Ericsson, L. E., "Loads Induced by Terminal-Shock Boundary Layer Interaction on Cone-Cylinder Bodies," *Journal of Spacecraft and Rockets*, Vol. 7, No. 9, Sept. 1970, pp. 1106–1112.

[19] Ericsson, L. E., Reding, J. P., and Guenther, R. A., "Launch Vehicle Gust Penetration Loads," *Journal of Spacecraft and Rockets*, Vol. 9, No. 1, Jan. 1972, pp. 19–25.

[20] Churchill, R. V., *Operational Mathematics*, 2nd ed., McGraw-Hill, New York, 1958.

[21] Gardner, M. F. and Barnes, J. L., *"Transients in Linear Systems,"* Vol. 1, Wiley, New York, Feb. 1956.

[22] Papadopoulus, J. G., "Wind Penetration Effects on Flight Simulation," AIAA Paper 67-609, Huntsville, Ala., 1967.

[23] Ericsson, L. E., Reding, J. P., and Guenther, R. A., "Relative Magnitudes of Stresses Caused by Static and Dynamic Launch Vehicle Loads," *Journal of Spacecraft and Rockets*, Vol. 10, No. 4, April, 1973, p. 276.